Search for negative U in the $Ba_{1-x}K_xBi_{1-y}Pb_yO_3$ system using constrained density-functional theory

G. Vielsack

Institut für Physik, Universität Dortmund, 44221 Dortmund, Federal Republic of Germany
and Fritz-Haber-Institut der Max-Planck-Gesellschaft, Faradayweg 4-6, 14195 Berlin/Dahlem, Federal Republic of Germany

W. Weber

Institut für Physik, Universität Dortmund, 44221 Dortmund, Federal Republic of Germany

Calculations using constrained density-functional theory have been carried out for the $Ba_{1-x}K_xBi_{1-y}Pb_yO_3$ system, using a full-potential linearized-augmented-plane-wave method and employing fcc supercell geometries with two formula units. The results have been mapped onto Hubbard-type models in order to extract values of interaction parameters U at the Bi sites. Two different mapping procedures have been utilized. The first one is the standard method, based on the comparison of total-energy curvatures. The second method, proposed in the present work, relies on the analysis of single particle energies and yields much smaller numerical errors. For $BaBiO_3$ interaction parameters are obtained for the following models: (i) s and p orbitals at Bi and p orbitals at O sites. Here, $U_s = 3.1 \pm 0.4$ eV, $U_{sp} = 1.4 \pm 0.2$ eV, $U_p = 2.2 \pm 0.4$ eV are found, (ii) s(Bi) and p(O) orbitals, yielding $U_s = 1.9 \pm 0.7$ eV, and (iii) an effective one-band model, leading to $U_s = 0.6 \pm 0.4$ eV. Further studies have been performed for breathing distorted $BaBiO_3$ and for various $Ba_{1-x}K_xBi_{1-y}Pb_yO_3$ alloys using virtual crystal approximations. The resulting U values are somewhat larger than for pure $BaBiO_3$. Thus, in all cases, the values of Bi U parameters are found to be positive. There is no indication of a negative U of electronic origin. [S0163-1829(96)05928-0]

I. INTRODUCTION

In Pb or alkali-doped $BaBiO_3$ with perovskite structure, high values of superconducting transition temperatures are observed, which extend up to 13 K for Pb-doped alloys and up to 30 K for K- or Rb-doped alloys.[1,2] Undoped $BaBiO_3$ is nonmetallic; here oxygen octahedra around the Bi ions exhibit alternating distortions of breathing-in and breathing-out type.[3] These distortions have been interpreted by chemists as charge disproportionations of the Bi^{4+} ions into either Bi^{5+} or Bi^{3+} ions. Some authors have attributed the apparent valence instability of Bi^{4+} to the presence of a ''negative U'' effect of atomic origin and have proposed that the large T_c values of doped $BaBiO_3$ are also caused by this feature.[4,5] In such a view, the $BaBiO_3$ system would be complementary to the cuprate superconductors, being a negative U Hubbard model system, while the cuprates represent manifestations of positive U Hubbard models.

In this paper we report on calculations to determine the values of U parameters of appropriate Hubbard-type models. In these calculations density-functional theory[6,7] is used and charge constraints are imposed on the valence electrons. The method of constrained density-functional theory (CDFT) is based on ideas of Gunnarsson and Lundqvist and has been generalized and first applied by Dederichs *et al.*[8,9] It has previously been used by Schlüter and co-workers and by other groups to determine U values in the case of cuprate superconductors.[10–13] The basic idea is to measure the change in the total energy, when charge at specific ions is ''elongated,'' i.e., enhanced or decreased, by imposing appropriate constraints. The curvatures of the CDFT total energy results are then mapped onto curvatures of the total-energy results obtained from Hubbard-type models where similar constraints are imposed.

The most important features of the electronic structure of $BaBiO_3$ are the wide conduction bands formed by hybridized O $2p_\sigma$ and Bi $6s$ orbitals.[14] The Fermi energy E_F is situated in the antibonding part of the band complex. Many nonbonding O $2p$ bands lie around $2–5$ eV below E_F. There is considerable admixture of Bi $6p$ orbitals in the conduction bands, especially at higher band energies. Thus an appropriate tight-binding Hamiltonian should include Bi $6s$, $6p$ and O $2p_\sigma$ orbitals. In principle, we are then able to determine values of both on-site interaction parameters U_s(Bi), U_p(Bi), U_{sp}(Bi), U_p(O), and of intersite parameters V_{sp}(Bi-O) and V_{pp}(Bi-O) for nearest neighbors and even for higher neighbors.

However, it is advantageous to keep any changes of the average ionic charges as small as possible — or else we would deal with a different chemistry. Therefore the constraints have to be imposed in an antisymmetric way, i.e., for atom A_1 of the super unit cell a charge reduction is imposed while for atom A_2 a corresponding charge increase is enforced. Moreover, there will be interactions of A_1 and A_2, because of the charge flow. Therefore, it is necessary to choose the two atoms A_1 and A_2 as far away from each other as possible. For U_p(O) as well as for the V parameters, these requirements can only be met using supercells of 4 to 8 formula units. Since we had to limit the cell size of the CDFT calculations to about 10 atoms/cell, only the U(Bi) parameters could be extracted.

The paper is organized as follows: In Sec. II, a short de-

scription of constrained density-functional theory is given. Two different procedures of mapping the CDFT results onto Hubbard-type models are presented in Sec. III. The basic density-functional calculations without constraints and their tight-binding analysis are reported in Sec. IV, the results of the CDFT calculations and of the mapping procedures are presented and discussed in Sec. V. Concluding remarks are given in Sec. VI.

II. CONSTRAINED DENSITY-FUNCTIONAL THEORY

In density-functional theory, the ground-state energy $\mathcal{E}_0$ is a functional $\mathcal{E}[\varrho]$ of the charge density ϱ, which is stationary with respect to any variation

$$\frac{\delta}{\delta \varrho} \left\{ \mathcal{E}[\varrho] - \mu \left(\int d^3 r \varrho(\mathbf{r}) - N \right) \right\} = 0. \quad (1)$$

Here we have imposed the constraint of a fixed number N of electrons, using the chemical potential μ as a Lagrangean multiplier. In order to enforce certain local charges N_i we can include additional constraints

$$\frac{\delta}{\delta \varrho} \left\{ \mathcal{E}[\varrho] - \mu \left(\int d^3 r \varrho(\mathbf{r}) - N \right) + \lambda_i \left(\int d^3 r \hat{P}_i \varrho(\mathbf{r}) - N_i \right) \right\}$$
$$= 0 \quad (2)$$

(the operators $\hat{P}_i$ will be specified below).

For our CDFT calculations we apply the local density approximation,[8] so that the variational scheme will lead to modified Kohn-Sham equations,

$$\left[-\frac{\Delta}{2} + v_H(\mathbf{r}) + v_{XC}[\varrho; \mathbf{r}] + \lambda_{il} \hat{P}_{il} \right] \chi_{k\mu}(\mathbf{r})$$
$$= \left[-\frac{\Delta}{2} + V_{SC}^\lambda + \lambda_{il} \hat{P}_{il} \right] \chi_{k\mu}(\mathbf{r}) = \varepsilon_{k\mu} \chi_{k\mu}(\mathbf{r}), \quad (3)$$

where v_H represents the ionic and Hartree parts, and v_{XC} the usual exchange-correlation part of the effective, self-consistent single-particle potential V_{SC}^λ — which also depends on the imposed constraints λ_{il} via charge redistribution effects. $\chi_{k\mu}(\mathbf{r})$ denotes the Kohn-Sham eigenstates of wave vector k and band index μ, which are linear combinations of appropriate basis functions ϕ_{k+G}:

$$\chi_{k\mu}(\mathbf{r}) = \sum_G c_G^{k\mu} \phi_{k+G}. \quad (4)$$

As we use the linear augmented plane-wave method (LAPW) local "charge elongations" can be generated only inside the muffin-tin spheres around the atomic sites. There, the Kohn-Sham equations have atomiclike solutions with wave functions ψ_{lm}^i. The projector $\hat{P}_{il}$ acts as a local potential $\lambda_{il} \hat{P}_{il}$ on ψ_{lm}^i. The muffin-tin part of the LAPW basis functions at site i is given by[15]

$$\phi_{\mathbf{k}_j}(\mathbf{r}) = \sum_{lm} \psi_{lm}^i = \sum_{lm} R_{lm}(|\mathbf{r} - \mathbf{R}_i|; E_l; \mathbf{k}_j) Y_{lm}(\hat{r}),$$

$$\mathbf{r} \in \text{muffin tin of site } i \quad (5)$$

and leads to the matrix elements

$$\langle \phi_{\mathbf{k}_j} | \hat{P}_{il} | \phi_{\mathbf{k}_{j'}} \rangle = \int_0^{R_i^{MT}} dr_i \, r_i^2 \sum_m$$
$$\times R_{lm}(r_i; E_l; \mathbf{k}_j)^* R_{lm}(r_i; E_l; \mathbf{k}_{j'}). \quad (6)$$

Above we have used the abbreviations $r_i := |\mathbf{r} - \mathbf{R}_i|$ and $\mathbf{k}_j := \mathbf{k} + \mathbf{G}_j$, where $\mathbf{G}_j$ is a reciprocal lattice vector.

The charge density is given by

$$\varrho(\mathbf{r}) = \sum_{k\mu} f_{k\mu} |\chi_{k\mu}(\mathbf{r})|^2 \quad (7)$$

with occupation numbers $f_{k\mu}$ of states $k\mu$. The total energy as a function of the local charge N_{il} is given by

$$\mathcal{E}(N_{il}) = \mathcal{E}[\varrho_{\lambda_{il}}] - \lambda_{il} \sum_k f_{k\mu} \int d^3 r \chi_{k\mu}^*(\mathbf{r}) \hat{P}_{il} \chi_{k\mu}(\mathbf{r}). \quad (8)$$

Here $\varrho_{\lambda_{il}}$ is the charge density as obtained under the constraint potential $\lambda_{il} \hat{P}_{il}$.

Actually, $\mathcal{E}(\lambda_{il})$ is computed instead of $\mathcal{E}(N_{il})$, which is obtained via the Legendre transformation

$$\mathcal{E}(N_{il}) = \mathcal{E}(\lambda_{il}) - \lambda_{il} N_{il}. \quad (9)$$

As $\mathcal{E}(N_{il})$ is determined by a variational procedure, it depends quadratically on the "charge elongations" $\delta N_{il} = N_{il} - N_{il}^0$ i.e.,

$$\mathcal{E}(\{N_{il}\}) = \mathcal{E}[\varrho_0] + \frac{1}{2} \sum_{il,i'l'} \widetilde{U}_{ll'}^{ii'} \delta N_{il} \delta N_{i'l'}. \quad (10)$$

It was pointed out by Hybertson et al.[10,11] that the coefficients $\widetilde{U}_{ll'}^{ii'}$ include all self-consistent charge redistribution effects. These effects have to be incorporated properly into the mapping procedures.

III. MAPPING PROCEDURES

A. Total-energy curvatures

In the Hubbard-type models, the local potentials $\lambda_{il} \hat{P}_{il}$ are assumed to act on atomiclike wave functions ψ_{lm}^i. The matrix elements equivalent to Eq. (6) lead to shifts of the orbital energies $\varepsilon_{il} \rightarrow \varepsilon_{il} + \lambda_{il}$, causing the "charge elongations" δn_{il}, which, in turn, may lead to further corrections of orbital energies and hopping terms. The values of the total energies $\mathcal{E}^{HM}(n_{il})$ are determined from mean-field solutions of the models. $\mathcal{E}^{HM}$ depends on the interaction parameters $U_{ll'}^{ii'}$, and so do the curvatures

$$\widetilde{u}_{ll'}^{ii'} = \frac{\partial^2 \varepsilon^{HM}}{\partial n_{il} \partial n_{i'l'}}. \quad (11)$$

However, we cannot simply equate $\widetilde{U}_{ll'}^{ii'}$ and $\widetilde{u}_{ll'}^{ii'}\{U\}$ for the determination of the interaction parameters $\{U\}$, as the charges δn_{il} of the Hubbard models and δN_{il} of the CDFT calculations are not identical. These quantities differ for two reasons: (i) the δN_{il} are restricted to the muffin-tin spheres, while the δn_{il} are not; (ii) the LAPW orbital basis is much larger and thus more flexible than the rather restricted tight-binding basis. For small "charge elongations," a linear dependence

$$\delta n_{il} = \sum_{i'l'} A_{ll'}^{ii'} \delta N_{i'l'} \qquad (12)$$

can be assumed. Knowing the matrix A, we can determine the $\{U\}$ values from the condition

$$\widetilde{U} \stackrel{!}{=} A^T \widetilde{u} \{U\} A. \qquad (13)$$

Note that the transformation matrix A is not equal to the matrix $\bar{A}$ transforming the full charges

$$n_{il} = \sum_{i'l'} \bar{A}_{ll'}^{ii'} N_{i'l'} \qquad (14)$$

as was assumed in Ref. 10. There, the LMTO method with overlapping muffin-tin spheres (and zero interstitial volume) has been used. Ratios $n_{il}/N_{il} \approx 1.1-1.3$ have been obtained, so that the approximation $A \approx \bar{A}$ may have been reasonable. We have found that for our LAPW calculations, where the interstitial volume is ≈ 0.65 of the total unit cell, the assumption $A \approx \bar{A}$ was not justifiable.

We have determined the elements of the A matrix from fits of tight-binding models to the energy bands of the CDFT-LAPW calculations. In these fits, only shifts of the orbital energies were used as adjustable quantities. Then, values of $\delta n_{il'}$ could be determined and compared to values of $\delta N_{il'}$. For our analysis we had to assume a site-diagonal matrix A, as we always have imposed antisymmetric ''charge elongations'' at the two Bi sites.

The model Hamiltonians are of the form

$$\hat{H} = \sum_{ll'ii'\sigma} T_{ll'}^{ii'} \hat{c}_{il\sigma}^\dagger \hat{c}_{i'l'\sigma} + \tfrac{1}{2} \sum_{ill'\sigma\sigma'}' U_{ll'} \hat{n}_{il\sigma} \hat{n}_{il'\sigma'}. \qquad (15)$$

Here, (i,i'), (l,l'), and (σ,σ') denote atomic sites, orbitals, and spins, respectively. $\hat{c}_{il\sigma}^\dagger$ is the electron creation operator and $\hat{n}_{il\sigma} = \hat{c}_{il\sigma}^\dagger \hat{c}_{il\sigma}$ is the corresponding number operator with $\langle \hat{n}_{il\sigma} \rangle = n_{il\sigma}$. The summation prime excludes the nonphysical $(l=l')$ $(\sigma=\sigma')$ term. We have $T_{ll'}^{ii} = \varepsilon_{il} \delta_{ll'}$. As the models include only Bi(s,p) and O(p) orbitals and since we have restricted ourselves to two inequivalent Bi sites per unit cell, we have only been able to consider the Bi on-site interaction parameters U_s, U_{sp}, and

$$U_p = \tfrac{1}{5} U_{p_x p_x} + \tfrac{4}{5} U_{p_x p_y}. \qquad (16)$$

In the mean-field approximation, the orbital energies ε_l are modified in the following way:

$$\varepsilon_s^{MF} = \varepsilon_s^0 + \tfrac{1}{2} U_s \langle \hat{n}_s \rangle + U_{sp} \langle \hat{n}_p \rangle, \qquad (17)$$

$$\varepsilon_p^{MF} = \varepsilon_p^0 + \tfrac{5}{6} U_p \langle \hat{n}_p \rangle + U_{sp} \langle \hat{n}_s \rangle.$$

Here $\langle \hat{n}_p \rangle = \Sigma_{\alpha\sigma} \langle \hat{n}_{p_\alpha\sigma} \rangle$. Charge ''elongations'' are induced by diagonal terms $\varepsilon_{il}^C = \lambda_{il}$, so that the mean-field Hamiltonian has the form

$$\hat{H}^{MF} = \sum_{ll'ii'\sigma} \{ [\varepsilon_{il}^{MF} + \lambda_{il}] \delta_{ii'} \delta_{ll'} + T_{ll'}^{ii'} (1-\delta_{ii'}) \} \hat{c}_{il\sigma}^\dagger \hat{c}_{i'l'\sigma}. \qquad (18)$$

$\mathcal{E}^{HM} = \langle \hat{H}^{MF} \rangle$ is found by self-consistent determination of the densities n_{il}.

B. Energy band analysis

Apart from total-energy values, the solutions of the Kohn-Sham equations contain a wealth of information on changes of energy bands, charge densities, and potentials under the action of the respective constraint. From these data, the U parameters can be extracted directly, without involving total-energy curvatures, and, in the case of the LAPW method, with the benefit of higher numerical accuracy.

The Kohn-Sham equations [Eq. (3)], which include the ''constraint'' potentials $\boldsymbol{\lambda}\hat{\mathbf{P}}$, induce ''charge elongations'' δN_{il} and thus a charge flow

$$\delta\varrho^\lambda = \varrho^\lambda - \varrho^{\lambda=0}, \qquad (19)$$

which results in a screening of the ''constraint'' potentials. In the Hubbard-type models, such a screening is purely determined by the interaction parameters $U_{ll'}$ — when we can justify that any changes of hopping terms can be ignored.

The self-consistent Kohn-Sham potentials of Eq. (3)

$$V^\lambda [\varrho^\lambda] = v_H^\lambda + v_{XC}^\lambda \qquad (20)$$

differ from the case $\lambda = 0$ by

$$\delta V^\lambda = V^\lambda - V^{\lambda=0}. \qquad (21)$$

When translated into mean-field solutions of the Hubbard-type models, the quantities δV^λ cause shifts $\delta\varepsilon_{il}(\delta V^\lambda)$ of orbital energies because of the changes $\delta n_{il'}$. The total shifts $\delta\varepsilon_{il}^\lambda$ are given by

$$\delta\varepsilon_{il}^\lambda = \lambda_{il} + \delta\varepsilon_{il}(\delta V^\lambda) \qquad (22)$$

$$= \lambda_{il} + \delta\varepsilon_{il}^{MF} \qquad (23)$$

With the help of Eq. (17) we now can determine the quantities $U_{ll'}$ from the variations

$$\frac{\delta\varepsilon_{il}^{MF}}{\delta n_{il'}} = C_{ll'} U_{ll'} \qquad (24)$$

with

$$C = \begin{pmatrix} 1/2 & 1 \\ 1 & 5/6 \end{pmatrix}. \qquad (25)$$

We can find $\delta\varepsilon_{il}^{MF}$ by analyzing the (non-self-consistent) Kohn-Sham equations

$$\left[-\frac{\Delta}{2} + V_{SC}^\lambda \right] \chi_{k\mu}^\lambda = \widetilde{\varepsilon}_{k\mu}^\lambda \chi_{k\mu}^\lambda, \qquad (26)$$

i.e., we carry out LAPW energy band calculations using only V_{SC}^λ, and then determine the changes $\delta\varepsilon_{il}^{MF}$ in another tight-binding analysis.

We have tried to estimate any changes of hopping terms due to δV^λ. This was done by allowing not only shifts of orbital energies, but also modifications of the $(sp\sigma)$ hoppings in the tight-binding fits. As will be discussed in some detail in Sec. IV, the magnitudes of certain gaps both in the

TABLE I. Atomic positions, muffin-tin radii (R_{MT}), and linearization energies E_l for $l=0$, 1, 2 of the valence and semicore (in parentheses) parts of the full potential LAPW calculations for sc BaBiO$_3$. The energies are given in Rydbergs and the positions in units of the sc lattice constant $a_0^{sc}=8.215$ bohrs.

	Position			R_{MT}	E_0	E_1	E_2
	x	**y**	**z**				
Ba	0.5	0.5	0.5	2.6345	-0.25(-1.49)	-0.32(-0.32)	0.30(-1.30)
Bi	0.0	0.0	0.0	2.2	-0.10(-0.10)	0.77(0.68)	-0.30(-1.23)
O	0.5	0.0	0.0	1.75	-0.72(-0.72)	0.30(0.00)	0.30(0.30)
	0.0	0.5	0.0				
	0.0	0.0	0.5				

bonding and antibonding parts of the Bi($6s$)O($2p_\sigma$) bands depend sensitively on the quantities $\Delta\varepsilon_s$(Bi) and $\Delta(sp\sigma)$. Our results give only very small values of $\Delta(sp\sigma)$. Qualitatively this result may be seen from the CDFT energy bands: there is always a much larger gap found for the bonding band than for the antibonding band (see Sec. IV). In effect, our approximations corresponds to using a site diagonal matrix A [Eq. (12)].

IV. LAPW CALCULATIONS WITHOUT CONSTRAINT AND THEIR TIGHT-BINDING ANALYSIS

In order to obtain the reference parameters for the tight-binding models underlying the respective Hubbard-type Hamiltonians, we first carried out full potential LAPW calculations for the BaBiO$_3$ system. For these computations, as well as for the CDFT ones, the WIEN full potential LAPW code[16] has been used. The implementation of the projectors $\hat{P}_i$ required certain changes in the FORTRAN code. In the WIEN code all core states are treated fully relativistically, while the valence and semicore states are calculated in the scalar-relativistic approximation. A ''two-window'' technique was used, where the Ba $5s$ and the Bi $6d$ states were calculated in a separate semicore ''window.'' Typical LAPW parameters are given in Table I.

Both simple cubic unit cells (for one formula unit) and face centered cubic unit cells (for two formula units per cell) have been considered, with typically $\approx$ 350 APW's (sc) and 700 APW's (fcc), respectively. 35 (20) k points in the irreducible Brillouin zone have been used for the iterations to self-consistency, which was typically achieved after $\approx$ 10 cycles. A small Fermi factor smearing of $\approx$ 2.5 meV was implemented to accelerate convergence.

A variety of calculations for the doped BaBiO$_3$ system have been performed. In the case of Ba$_{1-x}$Bi$_{2-y}$Pb$_y$O$_3$, the alloys were treated in the virtual crystal approximation (VCA). Similarly, in the case of alkali doping for Ba, the VCA was applied. As far as we could compare our results with those of previous calculations of other groups, very good agreement was found.

Our LAPW results were taken as the basis to extract matrix elements for various tight-binding models. A fit procedure very similar to the one described in Ref. 17 was used to obtain the model parameters. For all tight-binding models, an orthogonal basis was assumed, and, in general, the two-center approximation was applied.

For model I, both s and p orbitals on the Bi(Pb) atoms and p orbitals on the O have been included. The hopping

parameters were limited to atomic pair separations $d\le a$, the sc lattice constant. Model I is quite similar to one used by Mattheiss and Hamann[14,18] and similar model parameters were obtained. Note that we have distinguished between (1,0,0) type O-O hopping (via intermediate Bi) and (0,1,0) type O-O hopping (via the vacancy). This is the only deviation from the two-center approximation.

Typical rms values are approximately 0.14 eV. The rms deviations on the bonding and antibonding (Bi s) – (O p-σ) band complex are much smaller, of order 0.05 eV. The relatively large rms values arise from the nonbonding O p-π bands. We believe that these deviations are mainly caused by three-center effects in the nearest-neighbor O π-π hopping terms. The parameters of model I are given in Table II. It should be noted that they result in values n_s and n_p of Bi partial charges, which are in good agreement with the partial charges N_s and N_p inside the muffin-tin spheres of the

TABLE II. Tight-binding matrix elements of models I, II, and III for sc BaBiO$_3$ (in eV). The rms value of model I is $\approx$0.14 eV. In model II the matrix elements involving Bi p orbitals are set to zero, all others are retained from model I. In model III only the first and fourth nearest-neighbor (NN) Bi-Bi hopping matrix elements are nonzero. h_{pp} represents the crystal field splitting of the O p_σ and p_π orbitals.

''On-site'' matrix elements			
ϵ_s^{Bi}	ϵ_p^{Bi}	ϵ_p^{Ox}	$h_{pp}^{O\text{-}Bi}$
Model I			
-5.75	2.95	-2.60	-0.03
Bi-O 1NN hopping			
$(sp\sigma)$	$(pp\sigma)$	$(pp\pi)$	
2.22	2.64	-0.63	
O-O 1NN and 2NN hopping			
$(pp\sigma)^{(1)}$	$(pp\sigma)^{(2)}$		
0.40	0.28		
Bi-Bi 1NN hopping			
$(ss\sigma)$	$(sp\sigma)$	$(pp\sigma)$	$(pp\pi)$
-0.17	0.09	-0.33	0.33
Model III			
$(ss\sigma)$-1NN	$(ss\sigma)$-4NN		
-0.41	0.10		

TABLE III. Gradients of the tight-binding models I and II derived from breathing distorted LAPW calculations (A and B) and calculations with changed lattice constants (C). V and $\dot{V}$ give the values of the matrix elements for BaBiO$_3$ and their derivative, respectively, with respect to the doping x, within a linear least-square fit.

	BaPb$_x$Bi$_{1-x}$O$_3$					Fit		
	$x=1$	$x=0.75$	$x=0.5$	$x=0.25$	$x=0$	V_0	$\dot{V}$	rms
			A: breathing, model I					
$\epsilon_s^{\mathrm{Pb/Bi}}-\epsilon_p^{\mathrm{Ox.}}$	-1.62	-2.07		-2.03	-1.97	-2.05	0.26	0.14
$(sp\sigma)^{\mathrm{Bi/Pb\text{-}O}}$	-1.71	-2.10		-2.10	-1.93	-2.05	0.18	0.15
			B: breathing, model II					
$\epsilon_s^{\mathrm{Pb/Bi}}-\epsilon_p^{\mathrm{Ox.}}$	-1.92	-1.85	-1.78	-1.71	-1.64	-1.64	-0.28	0.01
$(sp\sigma)^{\mathrm{Bi/Pb\text{-}O}}$	-2.11	-2.02	-1.93	-1.84	-1.75	-1.75	-0.36	0.01
			C: lattice constant, model I					
$(sp\sigma)^{\mathrm{Bi/Pb\text{-}O}}$	-2.51	-2.64			-2.22	-2.25	-0.35	0.10
$(pp\sigma)^{\mathrm{Bi/Pb\text{-}O}}$	-1.35	-2.00			-2.03	-2.10	0.53	0.22

LAPW calculations. In particular, the ratios n_p/n_s and N_p/N_s are very similar.

In an extension of model I, also Ba s orbitals have been incorporated. These are expected to influence mainly the unoccupied conduction bands, as the LAPW results yield very small 6s orbital occupation within the Ba muffin-tin spheres. In the tight-binding model, a similarly small occupation of Ba s orbitals could only be achieved by placing the orbital energy $\varepsilon_s(\mathrm{Ba})$ far above $\varepsilon_p(\mathrm{Bi})$, so that the Ba s orbitals did not affect the main Bi-O bands. Note also that our model differs strongly from the tight-binding model of Ref. 19, where the Ba s orbital energy is much lower, while the Bi p orbital energy is moved to very high energies above E_F, resulting in very different partial charges.

Models II and III are simplified models. In model II, only Bi s and O p orbitals are used. As a consequence, none of the higher conduction bands is included in the model, also the top of the antibonding s-p band cannot be described correctly. Further, when distortions such as the breathing-type O displacements or Bi charge ''elongations'' are imposed, there is no flow of charge possible between Bi s and Bi p orbitals.

Model III represents an effective one-band model, where only the Bi s orbital is considered. Consequently, only the antibonding part of the s-p band complex can be described. The parameters of models II and III are also given in Table II.

As mentioned above, we have also performed LAPW calculations for breathing distorted BaBiO$_3$, using a fcc cell with the formula unit Ba$_2$Bi(I)Bi(II)O$_6$. Here, the Bi(I) site is surrounded by the contracted O octahedron (''breathing-in'' site with the formal valence $4+\delta$), while Bi(II) is the ''breathing-out'' site (formal valence $4-\delta$). Considerable band splittings are observed both in the bonding and the antibonding parts of the s-p band complex. Gaps appear especially along the L-W line of the fcc Brillouin zone. They are much wider in the antibonding band than in the bonding one. Further, orbital analysis of the LAPW results indicate that the center of mass of the Bi(I) 6s density has moved above the position of the L-W gaps, both for the bonding and

the antibonding bands. Correspondingly, the shifts of the Bi(II) 6s density occur in the opposite way. In Refs. 14 and 18, it was proposed to describe the band splittings solely by changes $\Delta(sp\sigma)$ in the $(sp\sigma)$ hopping $(sp\sigma)\rightarrow(sp\sigma)\pm\delta(sp\sigma)$. This assumption results in approximately equal L-W gaps for both bands. Moreover, the center of the Bi(I) bonding 6s density moves *below* the L-W gap position, since the Bi(I)-O $(sp\sigma)$ bonding states enhance their bonding character. In contrast, changes of the Bi 6s orbital energies $\varepsilon_s(\mathrm{Bi})\rightarrow\varepsilon_s(\mathrm{Bi})\pm\delta\varepsilon_s(\mathrm{Bi})$ result in an opposite shift of the 6s density in the bonding band, provided that $\delta\varepsilon_s>0$ for Bi(I).

We find that the two gradients $\delta(sp\sigma)$ and $\delta\varepsilon_s$ have approximately equal size, when $\delta\varepsilon_s$ is normalized per Bi-O bond. This leads to the smaller L-W gaps in the bonding bands and also constitutes the correct shifts of the 6s bonding density.

The tight-binding gradients derived from the LAPW calculation for breathing distorted configurations and from calculations with different lattice constants are given in Table III. The dependence of the tight-binding matrix elements on Pb doping is listed in Table IV.

V. CDFT CALCULATIONS AND THEIR ANALYSIS

A. General description

For our fcc supercell with two inequivalent Bi atoms, it is also possible to study changes of the U parameters under imposed O ''breathing'' distortions. The most general form of the ''constraint'' potential is given by

$$\boldsymbol{\lambda}\hat{\mathbf{P}}=\lambda_s(\hat{P}_s^{\mathrm{I}}-\hat{P}_s^{\mathrm{II}})+\lambda_p(\hat{P}_p^{\mathrm{I}}-\hat{P}_p^{\mathrm{II}}). \qquad (27)$$

When these constraint potentials are applied, the resulting charge flows occur mainly between Bi s and p orbitals and between Bi(I) and Bi(II) sites. The charge flow between Bi and O is very small; even for the biggest values of λ — which cause band gaps of several eV—the flow is of the order of 0.01e.

TABLE IV. Tight-binding matrix elements of model I for the $BaPb_xBi_{1-x}O_3$ system (in eV). The rms of the least-square fit to the LAPW bands is ≈ 0.14 eV. V and $\dot{V}$ give the values of the matrix elements for $BaBiO_3$ and their derivative, respectively, with respect to doping x, using a linear least-square fit.

| | $BaPb_xBi_{1-x}O_3$ | | | | | Fit | | |
	$x=1$	$x=0.75$	$x=0.5$	$x=0.25$	$x=0$	V_0	$\dot{V}$	rms
$\epsilon_s^{Pb/Bi} - \epsilon_p^{Ox.}$	-0.87	-1.48	-1.99	-2.61	-3.20	-3.19	2.32	0.01
$\epsilon_p^{Pb/Bi} - \epsilon_p^{Ox.}$	6.99	7.15	6.51	5.78	5.55	5.55	1.69	0.09
$h_{pp}^{O-Pb/Bi}$	0.16	0.06	0.01	0.04	-0.03	-0.03	0.16	0.05
	Pb/Bi-Pb/Bi 1NN hopping							
$(ss\sigma)$	-0.13	-0.15	-0.15	-0.16	-0.17	-0.17	0.04	0.01
$(sp\sigma)$	0.08	0.08	0.10	0.06	0.10	0.09	-0.01	0.08
$(pp\sigma)$	-0.53	-0.11	-0.21	-0.37	-0.40	-0.33	0.00	0.07
$(pp\pi)$	0.30	0.42	0.37	0.31	0.32	0.33	0.03	0.02
	Pb/Bi-O 1NN hopping							
$(sp\sigma)$	2.12	2.13	2.17	2.19	2.22	2.22	-0.10	0.00
$(pp\sigma)$	2.57	2.68	2.71	2.63	2.60	2.64	0.01	0.02
$(pp\pi)$	-0.59	-0.63	-0.57	-0.62	-0.64	-0.63	0.03	0.01
	O-O 1NN hopping							
$(pp\sigma)$	0.35	0.37	0.38	0.38	0.40	0.40	-0.04	0.00
	O-O 2NN hopping							
$(pp\sigma)$	0.19	0.13	0.21	0.27	0.28	0.28	-0.15	0.01
E_F	0.99	1.87	2.35	2.56	2.59			
$\mathcal{N}_\uparrow(E_F)$	0.96	0.13	0.21	0.32	0.51			

We have studied four classes of constraint potentials [Eq. (27)]: (1) $\lambda_s > 0$, $\lambda_p = 0$. This case leads to a flow ΔN_s from Bi(I) to Bi(II) and to a smaller backflow ΔN_p. [For the remaining part differences of physical quantities between the Bi(I) and Bi(II) site are denoted by Δ.] (2) $\lambda_s = 0$, $\lambda_p > 0$. Here we get a flow ΔN_p from I to II and some backflow ΔN_s. (3) $\lambda_s = \lambda_p > 0$ leads to flows ΔN_s and ΔN_p from I to II. (4) $\lambda_s = -\lambda_p > 0$ leads to flow ΔN_s from I to II and a backflow ΔN_p.

For each class of potential, at least three different values of λ_s or λ_p up to $\lambda_{s,p} = 0.25$ Ry have been evaluated. The classes (3) and (4) have been included to better determine the bilinear coefficients $(\Delta N_s)(\Delta N_p)$ on the total-energy surface. Typical values of ΔN_s, ΔN_p, etc. for $\lambda_{s,p} = 0.15$ Ry are given in Table V. The ''muffin-tin'' partial densities of states for a calculation using $\lambda_s = 0.2$ Ry and $\lambda_p = 0$ are shown in Fig. 1.

B. Analysis of the CDFT total energies

We may express the total-energy surface in the space of ΔN_s and ΔN_p by

$$\Delta \mathcal{E} = \widetilde{U}_s (\Delta N_s)^2 + \widetilde{U}_p (\Delta N_p)^2 + \widetilde{U}_{sp} \Delta N_s \Delta N_p . \quad (28)$$

The quantities $\widetilde{U}_s$, $\widetilde{U}_p$, and $\widetilde{U}_{sp}$ are found by a least-squares fit to approximately 15 values of $\Delta \mathcal{E}$ (rms deviation ≈ 3

meV). We find $\widetilde{U}_s = 4.7$ eV, $\widetilde{U}_p = 9.0$ eV, and $\widetilde{U}_{sp} = 5.1$ eV. Figure 2 shows a typical $\Delta \mathcal{E}$ versus ΔN_s curve. Note that the curvature does *not* yield $\widetilde{U}_s$, as $\lambda_s \neq 0$ also includes finite ΔN_p values.

The numerical convergence of the total-energy values was tested by using larger numbers of APW's, increasing the number of k points from 20 to 89, and replacing the Fermi factor smearing by a tetrahedral integration scheme in order to increase the accuracy of the state occupation numbers. All these tests did not lead to any significant changes in the

TABLE V. Bi s and Bi p muffin-tin LAPW (ΔN) and tight-binding (Δn) charge transfers obtained from the CDFT calculations and the corresponding tight-binding analysis. Antisymmetric constraint potentials $\boldsymbol{\lambda}\hat{\mathbf{P}} = \lambda_s(\hat{P}_s^I - \hat{P}_s^{II}) + \lambda_p(\hat{P}_p^I - \hat{P}_p^{II})$ were applied at the Bi site. The changes in the total energy $\Delta \mathcal{E}$ are given in mRy.

| | (λ_s, λ_p) | | | |
	(0.15,0.00)	(0.00,0.15)	(0.15,0.15)	(0.15,-0.15)
	CDFT			
ΔN_s	0.27	-0.06	0.19	0.32
ΔN_p	-0.07	0.14	0.07	-0.21
$\Delta \mathcal{E}$	21.3	10.3	20.6	38.8
	Tight-binding			
Δn_s	0.46	-0.16	0.38	0.55
Δn_p	-0.12	0.32	0.21	-0.45
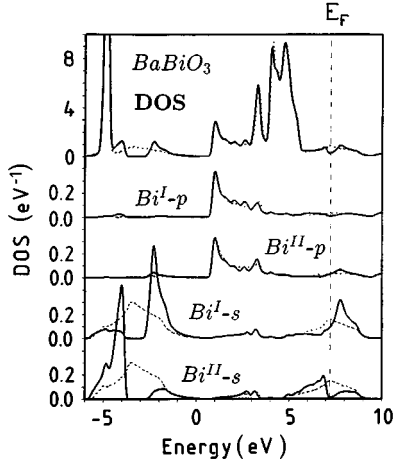
FIG. 1. LAPW muffin-tin DOS and partial DOS obtained by an antisymmetric constraint potential with $\lambda_s = 0.2$ Ry and $\lambda_p = 0$. For comparison the DOS from calculations *without* constraint potential is also shown (dashed lines).

curvature values ($\lesssim 1$–2 %). Consequently we estimate the error of the $\widetilde{U}$ values to be $\approx 2\%$.

The crucial point of the analysis is the scaling of the respective flows of LAPW muffin-tin and tight-binding charges. It turns out that the total charges N_l (LAPW) and n_l (tight binding) scale in a different manner than do the differential charges ΔN_l and Δn_l. By adjusting the effective orbital energies in the tight-binding models to the energy bands of the CDFT calculations, we are able to determine the Δn_l values as functions of the ΔN_l. Typical relations between Δn_l and ΔN_l are shown in Fig. 3. Note again that Δn_l does not only depend on ΔN_l, but also on $\Delta N_{l'}$, so that the slopes do not directly translate into elements of the scaling matrix $A_{ll'}$.

In a good approximation, a linear scaling is found, and we obtain for the scaling matrix [Eq. (12)]

$$\mathbf{A} = \begin{pmatrix} 1.86 & 0.16 \\ 0.15 & 2.40 \end{pmatrix}. \qquad (29)$$

The error in the diagonal matrix elements of $\mathbf{A}$ turns out to be of the order $\approx \pm 0.2$–0.3. Using $\mathbf{A}$, we can replace
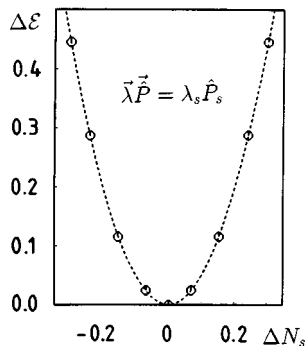
FIG. 2. CDFT total energy as a function of the Bi s charge transfer ΔN_s resulting from calculations with $\lambda_s > 0$ and $\lambda_p = 0$.
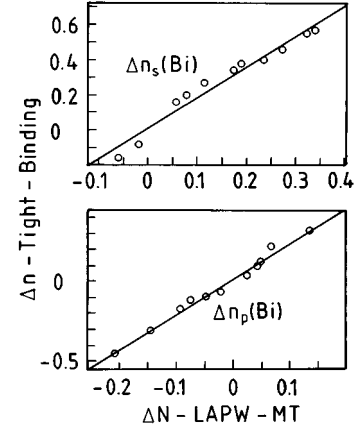
FIG. 3. Bi s and p charge transfers Δn_s and Δn_p obtained from the tight-binding analysis as functions of the corresponding muffin-tin CDFT-LAPW charge transfers ΔN_s and ΔN_p.

$\Delta\mathcal{E}(\Delta\mathbf{N})$ by $\Delta\mathcal{E}(\Delta\mathbf{n})$. Note that $\mathbf{A}$ enters quadratically the expression for U_i. This leads to a large enhancement of errors in the U values.

Next we determine the corresponding total-energy changes in the Hubbard-type models in mean-field approximation. Again we may write

$$\Delta\mathcal{E}^{\mathrm{MF}} = \widetilde{U}_s^{\mathrm{HM}} \Delta n_s^2 + \widetilde{U}_p^{\mathrm{HM}} \Delta n_p^2 + \widetilde{U}_{sp}^{\mathrm{HM}} n_s n_p \qquad (30)$$

The curvatures $\widetilde{U}_i^{\mathrm{HM}}$ are functions of the Hubbard parameters U_s, U_p, and U_{sp}. By equating $\widetilde{U}_i^{\mathrm{CDFT}} = \widetilde{U}_i^{\mathrm{HM}}$ we can finally determine U_s, U_p, and U_{sp}. We find $U_s = 3.1 \pm 1$ eV, $U_p = 1.7 \pm 1$ eV, and $U_{sp} = 1.2 \pm 1$ eV. For the ''bare'' orbital energies ε_i^0 we have thereby obtained $\varepsilon_s^0 = \varepsilon_p^0 - 6.8$ eV, $\varepsilon_p^0 = \varepsilon_p(\mathrm{O}) + 2.2$ eV.

When we try to map the CDFT results on models II and III, there is the problem, whether and how to include the backflow in the LAPW p channel. This gives some more ambiguity to the results. For the analysis, only class (1) constraints have been used. For model II, we find $U_s = 1.0$–2.5 eV, with $A_{ss} = 1.4$–1.8, while for model III (effective one-band model) we get $U_s = 0.2$–1.5 eV, with $A_{ss} = 3.0$–4.5 eV.

C. Results of energy band analysis

As discussed in Sec. III B, there is an alternate way of extracting the U parameters from the analysis of the one-particle energy bands. Both the bands of the CDFT calculations are needed — here the tight-binding analysis leads to the values of the charge flows Δn_l — and the bands obtained from the Kohn-Sham equations [Eq. (26)] — here the shifts of orbital energies $\Delta\varepsilon_l$ caused by the potential changes due to the charge flows are extracted.

Figure 4 exhibits typical CDFT energy bands, with large band gaps, especially in the bonding part of the s-p bands. These gaps are mainly caused by the ''constraint'' potential $\lambda\hat{\mathbf{P}}$, which also induces the flow of charge in the s and p channels as seen in the partial densities of states curves (see also Fig. 1). The bands obtained by solving Eq. (26) (see Fig. 5) illustrate the role of the screening potential $\Delta V_{\mathrm{SC}}^\lambda$, induced by the charge flows. The band gaps are much smaller, and the partial density of states curves indicate that, when
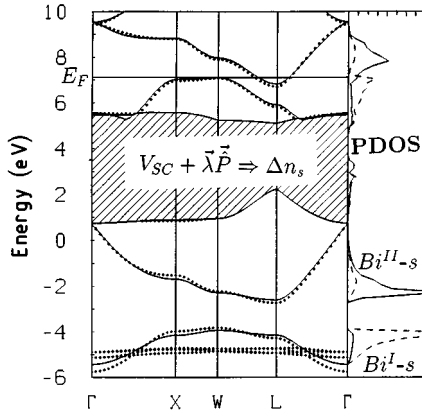
FIG. 4. Energy bands of the CDFT calculations for BaBiO$_3$ with antisymmetric constraint potential $\lambda_s(\hat{P}_s^{\mathrm{I}}-\hat{P}_s^{\mathrm{II}})$ and $\lambda_s=0.2$ Ry. The dotted lines show the LAPW bands and the full lines the corresponding tight-binding bands. In the right pannel of the figure the Bi(I) and Bi(II) s partial DOS from the tight-binding analysis are shown.

$\Delta V_{\mathrm{SC}}^{\lambda}$ is taken without $\boldsymbol{\lambda}\hat{\mathbf{P}}$, the resulting charge would flow back towards the equilibrium situation. The tight-binding analysis yields the shifts of the orbital energies $\Delta\varepsilon_l^{\mathrm{MF}}$, caused by the action of $\Delta V_{\mathrm{SC}}^{\lambda}$, which can be related to the Δn_l and to the U parameters:

$$\Delta\varepsilon_s^{\mathrm{MF}}=\tfrac{1}{2}\,U_s\Delta n_s+U_{sp}\Delta n_p, \tag{31}$$

$$\Delta\varepsilon_p^{\mathrm{MF}}=\tfrac{5}{6}\,U_p\Delta n_p+U_{sp}\Delta n_s. \tag{32}$$

The approximately linear relation between $\Delta\varepsilon_l^{\mathrm{MF}}$ and Δn_l is illustrated in Fig. 6. Simply analyzing the slope in Fig. 6 and thus neglecting the Δn_p contributions leads to an approximate U_s value of 2.8 eV.

For a complete analysis, all 15 CDFT calculations have been evaluated. The following values are found: $U_s=3.1\pm0.4$ eV, $U_p=2.2\pm0.4$ eV, and $U_{sp}=1.4\pm0.2$ eV. These numbers have considerably smaller numerical errors than those obtained from the total-energy analysis.
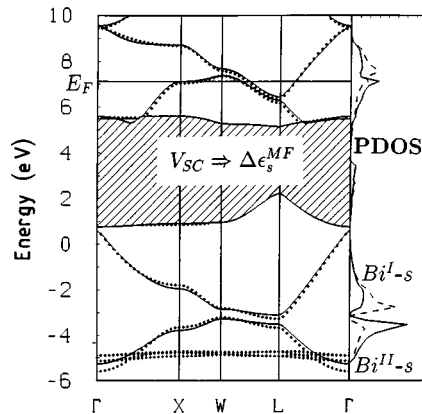
FIG. 5. Energy bands calculated with $V_{\mathrm{SC}}^{\lambda}$ but without the constraint potential [Eq. (26)]. The dotted lines show the LAPW bands and the full lines the corresponding tight-binding bands. In the right pannel of the figure the Bi s partial DOS from the tight-binding analysis are shown.
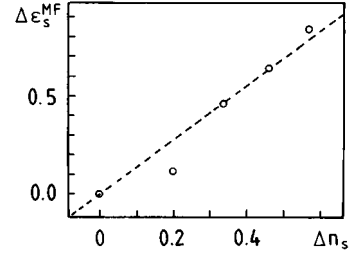
FIG. 6. Simplified analysis of the tight-binding energy bands: $\Delta\epsilon_s^{\mathrm{MF}}$ is shown as a function of Δn_s. The slope gives an estimate of the U_s value.

For models II and III, similar procedures have been carried out. The same ambiguities as discussed in Sec. V B are valid here. Therefore, the values for U_s exhibit much larger spreads. For model II, we find $U_s=1.3$–2.5 eV, for model III, $U_s=0.2$–1.0 eV. In spite of the bigger spread of the numbers, there are no indications for negative U values.

D. Values of U parameters for "breathing" distorted BaBiO$_3$

In "breathing" distorted Ba$_2$Bi(I)Bi(II)O$_6$, the two Bi atoms are inequivalent and may carry quite different ionic charges. Consequently, the values of U parameters may change from the undistorted case. In particular, terms due to first order in displacement are possible and may be important.

Again we study the changes of charge densities δn and of effective orbital energies $\delta\varepsilon^{\mathrm{MF}}$ under constraints and now, also under oxygen breathing distortions η. We write

$$\delta\epsilon_s^{\mathrm{MF}}=\tfrac{1}{2}\,(U_s^0+U_s'\eta+U_s''\eta^2+\cdots)\delta n_s+$$

$$(U_{sp}^0+U_{sp}'\eta+U_{sp}''\eta^2+\cdots)\delta n_p+$$

$$6V_{CR}^{s'}\eta+\cdots. \tag{33}$$

Here, U_s and U_{sp} are considered up to η^2. $V_{CF}^{s'}$ is a crystal field derivative, caused by the shift of the oxygen potentials acting on the Bi s orbitals. It is important to note that any changes in the U values linear in η move the center-of-mass value

$$\delta\bar{\epsilon}_s^{\mathrm{MF}}:=\tfrac{1}{2}\,[\,\delta\epsilon_s^{\mathrm{MF}}(\mathrm{I})+\delta\epsilon_s^{\mathrm{MF}}(\mathrm{II})\,]$$

$$=(\tfrac{1}{4}\,U_s'\Delta n_s^0+\tfrac{1}{2}\,U_{sp}'\Delta n_p^0)\,\eta+O(\eta^2), \tag{34}$$

where $\Delta n_i^0=1/2(\delta n_i^{\mathrm{I}}-\delta n_i^{\mathrm{II}})$, relative to the oxygen p level. Assuming a value of $\eta=0.035$ Å (which is close to the mini-

TABLE VI. Change of the center of mass of the Bi s on-site energies (given in eV) of the tight-binding analysis due to breathing distortion ($\eta=\delta d_{\mathrm{Bi\text{-}O}}=0.035$ Å) and antisymmetric constraint potentials (given in Ry) with $\lambda_p=0$. Also shown are the s charge transfers Bi$^{\mathrm{I}}\rightarrow$ Bi$^{\mathrm{II}}$ Δn_s^0, and Δn_p^0, respectively.

$\lambda_s=$	0.2	0.1	0	-0.1	-0.2
$\delta\bar{\epsilon}_s^{\mathrm{MF}}$	0.04	0.01	0.00	-0.01	-0.01
Δn_s^0	0.76	0.63	0.40	0.16	-0.26
Δn_p^0	-0.14	-0.10	0.02	0.12	0.18

TABLE VII. Values of U parameters (in eV) for Bi for the breathing distortion $\eta = 0.035$ Å. Also listed are the "unscreened" gradients of the crystal field parameters $V_{CF}^{s\prime}$ and $V_{CF}^{p\prime}$.

	U_s	U_p	U_{sp}	$V_{CF}^{s\prime}$	$V_{CF}^{p\prime}$
(a)	3.5 ± 0.4	2.5 ± 0.4	1.7 ± 0.2	-4.4 ± 0.2	-1.7 ± 0.2
(b)	3.8 ± 1.0	2.5 ± 1.0	1.9 ± 1.0		

mum of the frozen phonon calculations[20–22]) we have carried out various constrained calculations. The results concerning the center-of-mass shifts $\delta\bar{\varepsilon}_s$ are summarized in Table VI. Although considerable charge density variations occur, there is hardly any change in the center-of-mass values $\delta\bar{\varepsilon}_s$. The only values of U_s' and U_{sp}' compatible with Eq. (34) are $U_s' = U_{sp}' \approx 0$. We thus conclude that within our numerical accuracy of approximately 0.02 eV/Å , there is no linear dependence of the U parameters on distortions.

Further analysis of the constrained calculations yield U values as given in Table VII. Both methods of analysis give very similar numbers, which are somewhat larger than the values for undistorted BaBiO$_3$.

E. Dependence of the U parameters on band filling

Within virtual crystal approximation, we have also carried out constrained calculations for a variety of alloys, with the goal to study the dependence of the U parameters on the filling of the antibonding Bi($6s$)-O($2p\sigma$) band. The band filling is modified either by assuming a noninteger nuclear charge on the Bi site, ranging between $Z_{eff}=82.25 = (\text{Pb}_{0.75}\text{Bi}_{0.25})$ to $Z_{eff}=83.5=(\text{Bi}_{0.5}\text{Po}_{0.5})$, or by modifying the nuclear charge on the Ba site. The constrained calculations have focused on the values of U_s, i.e., in all calculations we have put $\lambda_p=0$. Only one constrained calculation per alloy was performed and analyzed using the energy band method. Thus the statistical errors of the U_s values are somewhat larger than in the full analysis of BaBiO$_3$. The main results of the alloy calculations are listed in Table VIII.

Interestingly, there is a significant parabolic variation of U_s with band filling (see also Fig. 7), which is beyond the statistical errors. We interpret these results as caused by the interactions of the charge "elongations" at the two different Bi sites of our fcc superlattice. The latter corresponds to a Bi(I)-Bi(II) ordering wave of wave vector $\mathbf{Q}=\pi/a(111)$, the $\mathbf{R}$ point of the sc Brillouin zone. The bare conduction-band susceptibility

TABLE VIII. Analysis of CDFT calculations for the $\text{Ba}_{1-x}\text{K}_x\text{Bi}_{1-y}\text{Pb}_y\text{O}_3$ system using the band analysis method. The CDFT calculations were performed with $\lambda_s=0.2$ Ry and $\lambda_p=0$. $n_s(x)-n_s^0$ gives the change of the Bi s partial occupation referred to the undoped BaBiO$_3$, obtained without constraint.

	$\Delta\epsilon_s^{MF}$	Δn_s	$n_s(x)-n_s^0$	$U_s=2\Delta\epsilon_s^{MF}/\Delta n_s$
$\text{BaPb}_{0.75}\text{Bi}_{0.25}\text{O}_3$	0.57	0.22	-0.33	5.2
$\text{Ba}_{0.5}\text{K}_{0.5}\text{BiO}_3$	0.55	0.27	-0.27	4.1
$\text{BaPb}_{0.5}\text{Bi}_{0.5}\text{O}_3$	0.53	0.31	-0.21	3.4
BaBiO_3	0.84	0.57	0.0	2.9
$\text{BaBi}_{0.5}\text{Po}_{0.5}\text{O}_3$	0.37	0.17	0.23	4.4
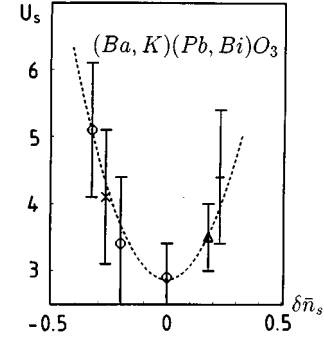
FIG. 7. Dependence of the U_s value at the Bi/Pb/Po site on the change of the respective partial s charge $\delta\bar{n}_s := n_s-n_s^0$. Here n_s^0 represents the value of the Bi s charge of undistorted BaBiO$_3$. Also shown is the U_s value of breathing distorted BaBiO$_3$ ($\delta d_{\text{Bi-O}}=0.035$ Å). The dashed line illustrates the quadratic behavior of the electronic susceptibility $\chi_{\mathbf{Q}}^{-1}$ for $\mathbf{Q}=\pi/a(1,1,1)$ as a function of Pb or Po doping.

$$\chi_{\mathbf{Q}} = \sum_{\mathbf{k}} \frac{f_{\mathbf{k}}-f_{\mathbf{k}+\mathbf{Q}}}{\varepsilon_{\mathbf{k}}-\varepsilon_{\mathbf{k}+\mathbf{Q}}} \qquad (35)$$

exhibits a large maximum at the half-filled case, so that the interatomic screening of the charge elongations should be largest there. This effect shows up in a parallel behavior of U_s and $\chi_{\mathbf{Q}}^{-1}$ as a function of band filling (see Fig. 7). We expect that for constrained calculations using supercells where the $\mathbf{Q}=\pi/a(111)$ vector is not involved, the U_s values for undoped BaBiO$_3$ should also increase.

F. Discussion of the results

In all three Hubbard-type models for BaBiO$_3$, the interaction parameters are positive. In particular, model I, the most extended model with Bi s and p, and O p_σ orbitals, exhibits a value of $U_s \approx 3$ eV. There, the intra-atomic screening of the constraint potentials occurs in an analogous way as in the LAPW results, i.e., as a charge flow between Bi s and p charge density. In model II, where only Bi s and O p_σ orbitals are present, a somewhat smaller value of $U_s \approx 2$ eV is found. We think that the removal of the Bi p channel results in a more strongly screened U_s. In model III, an effective one-band model, a further reduction of U_s to values ≈ 0.8 eV, is obtained. For model III, the constraint potentials produce very large inter-atomic charge flows, mainly because of the small bandwidth of the antibonding part of the Bi(s)-O(p_σ) bands, which results in an effective hopping of only ≈ 0.7 eV. In neither case, however, are indications for a negative U_s found.

The CDFT calculations for breathing distorted BaBiO$_3$ give two important results. First, any component U_s', linear in the breathing distortion η, is vanishingly small [U_s' should lead to an asymmetry in the U_s values of Bi(I) and Bi(II)]. Second, there is a considerable change of U_s on both Bi sites, i.e., quadratic in η. The CDFT results for various alloys also indicate increases of U_s, now quadratic in the deviation from the half-filled band case. We believe, therefore, that the half-filled band case of BaBiO$_3$ is special, because of strong interactions of the Bi(I)-Bi(II) "charge elongations" due to strong nesting features.

Thus we think that the U values for pure $BaBiO_3$ are, indeed, a lower limit for the system, and we expect that CDFT calculations employing larger supercells will lead to a bigger value of U_s.

VI. CONCLUDING REMARKS

In this paper, we have carried out calculations using constrained density-functional theory with the goal of obtaining reliable estimates for the interaction parameters U_s, U_{sp}, and U_p of Hubbard-type models for the $BaBiO_3$ system.

For our calculations we have employed the full-potential linear-augmented plane-wave scheme. The results have been mapped onto appropriate Hubbard-type models by two different methods. The first one was used previously for cuprate calculations and is based on the analysis of total-energy curvatures and a mapping of the charge density variations within the muffin-tin atomic spheres onto thoses of appropriate tight-binding models. The second method, which to our knowledge is presented here for the first time, is based on an analysis of the two different kinds of single-particle energies, one obtained from the total self-consistent potentials with constraints, the other from the potentials without constraint, but including the self-consistent responses to the constraints. With this method, a more direct access to the values of the U parameters is achieved, resulting in much smaller numerical errors. Actually we do not see a principal reason why the second method has to be restricted to energy band schemes employing a muffin-tin separation of atomic and interstitial charges. It is conceivable to even use pseudopotential schemes with a plane-wave basis for the evaluation of interaction parameters.

Due to computational limitations, only a fcc supercell with two formula units could be studied. As a consequence, only U parameters at Bi sites could be extracted.

Three different Hubbard-type models have been investigated. The first and most complex model employs s and p orbitals at Bi sites and p orbitals at the O sites. In model I, three interaction parameters U_s, U_{sp}, and U_p have been extracted. We find $U_s = 3.1 \pm 0.4$ (3.1 ± 1) eV, $U_{sp} = 1.4 \pm 0.2$ (1.2 ± 1) eV, $U_p = 2.2 \pm 0.4$ (1.7 ± 1) eV; thereby the values in brackets result from the total-energy analysis. In model II, only s (Bi) and p_σ (O) orbitals are considered. Here, no intra-atomic screening of the constraint potentials is possible, resulting in a lower value of $U_s = 1.3 - 2.5$ ($1.0 - 2.5$) eV. For the effective one-band model III, even lower values $U_s = 0.2 - 1.0$ ($0.2 - 1.5$) eV are found.

Further CDFT calculations for breathing distorted $BaBiO_3$ and for a variety of alloys indicate that the U values for $BaBiO_3$ are a lower limit. Therefore we conclude that there is no evidence for a negative U at Bi atoms, which is of electronic origin.

[1] D. E. Cox and A. W. Sleight, Solid State Commun. **19**, 969 (1976).

[2] L. F. Mattheiss, E. M. Gyorgy, and D. W. Johnson, Jr., Phys. Rev. B **37**, 3745 (1988); R. J. Cava *et al.*, Nature (London) **332**, 814 (1988).

[3] D. E. Cox and A. W. Sleight, Acta Crystallogr. B **35**, 1 (1979); in *Proceedings of the Conference on Neutron Scattering, Gatlinburg, 1976,* edited by R. M. Moon (National Technical Information Service, Springfield, VA, 1976), pp. 45–54.

[4] C. M. Varma, Phys. Rev. B **61**, 2713 (1988).

[5] D. Yoshioka and H. Fukuyama, J. Phys. Soc. Jpn. **54**, 2996 (1985).

[6] P. Hohenberg and W. Kohn, Phys. Rev. **136**, B864 (1964).

[7] W. Kohn and L. J. Sham, Phys. Rev. **140**, A1133 (1965).

[8] O. Gunnarsson and B. I. Lundqvist, Phys. Rev. B **13**, 4274 (1976).

[9] P. H. Dederichs, S. Blügler, R. Zeller, and A. Akai, Phys. Rev. Lett. **53**, 2512 (1984).

[10] M. S. Hybertson, M. Schlüter, and N. E. Christensen, Phys. Rev. B **39**, 9028 (1989).

[11] M. S. Hybertson and M. Schlüter, in *New Horizons in Low Dimensional Electron Systems*, edited by M. Levy *et al.* (Kluwer Academic, Dordrecht, 1992).

[12] A. K. McMahan, R. M. Martin, and S. Satpathy, Phys. Rev. B **38**, 6650 (1988).

[13] O. Gunnarsson, O. K. Andersen, O. Jepsen, and J. Zaanen, Phys. Rev. B **39**, 1708 (1989).

[14] L. F. Mattheiss and D. R. Hamann, Phys. Rev. B **28**, 4227 (1983).

[15] See, for example, D. D. Koelling, and G. O. Arbman, J. Phys. F **5**, 2041 (1975), and citations therein.

[16] P. Blaha, K. Schwarz, P. Sorantin, and S. B. Trickey, Comput. Phys. Commun. **59**, 399 (1990).

[17] L. F. Mattheiss and W. Weber, Phys. Rev. B **25**, 2248 (1982).

[18] L. F. Mattheiss, Jpn. J. Appl. Phys. Suppl. **24-2**, 6 (1985).

[19] D. A. Papaconstantopoulos, A. Pasturel, J. P. Julien, and F. Cyrot-Lackmann, Phys. Rev. B **40**, 8844 (1989).

[20] P. Blaha, K. Schwarz, G. Vielsack, and W. Weber in *Electronic Properties of High-T_c Superconductors and Related Compounds*, edited by H. Kuzmany, M. Mehring, and J. Fink (Springer, Berlin, 1990).

[21] A. I. Liechtenstein, I. I. Mazin, C. O. Rodriguez, O. Jepsen, O. K. Andersen, and M. Methfessel, Phys. Rev. B **44**, 5388 (1991).

[22] K. Kunc, R. Zeyher, A. I. Liechtenstein, M. Methfessel, and O. K. Andersen, Solid State Commun. **80**, 325 (1991).